THE JOURNAL OF PHYSICAL CHEMISTRY C
A JOURNAL OF THE AMERICAN CHEMICAL SOCIETY

pubs.acs.org/JPCC

Article

Ester-Carbene and Its Dimerization with Exclusive *Cis*-Selectivity on a Silver Surface

Chia-Hung Wu, Jean-Ho Chu, Chih-Hung Chou, Po-Chiao Lin, Chi-Wi Ong,* and Chao-Ming Chiang*

Cite This: *J. Phys. Chem. C* 2022, 126, 2482−2492

Read Online

ACCESS | Metrics & More | Article Recommendations | Supporting Information

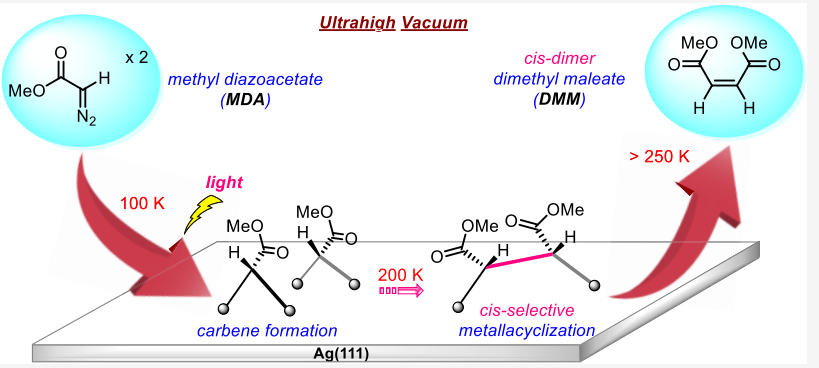

ABSTRACT: Diazo compounds are key precursors to carbenes. Here, methyl diazoacetate is dosed onto an Ag(111) surface and subjected to 365 nm UV light activation. Loss of N_2 generates a metastable metal-bonded methyl ester-carbene at 100 K, which is confidently diagnosed using reflection−absorption infrared spectroscopy in conjunction with the theoretically calculated frequencies, intensities, and normal modes, corroborating the structure assignments. To the best of our knowledge, this is the first synthesis of extended surface-based ester-carbene and its capture. Upon annealing the surface at 200 K, part of the neighboring ester-carbene species are well positioned to undergo intraoverlayer dimerization and afford preferentially *cis*-configured alkene (maleate). We thus demonstrate the efficient formation of thermodynamically less stable, isomerically pure *cis*-alkenes via a surface-mediated process. In addition to dimerization, heating Ag(111) to 200 K induces selective C−O bond cleavage of the methyl ester-carbene to yield methoxy and ketenyl fragments, which eventually yield formaldehyde, methanol, and ketene as gas-phase products above 300 K. In contrast, no trace Wolff rearrangement, the reaction characteristic of diazo carbonyl compounds, is observed. Remarkable stereoselectivity and chemoselectivity are demonstrated, and this work showcases how a silver surface can act to accommodate carbenes and allows the characterization of reactive intermediates usually seen only in matrices.

INTRODUCTION

In contrast to tetravalent carbon compounds, divalent carbon species (carbenes) are unusual, energetic, reactive forms of carbon; thus, they are often considered too short-lived for isolation and direct characterization. The coordination of such unstable species to transition-metal surfaces has been a useful tactic in studying their roles in heterogeneous catalytic transformations or harnessing their reactivity for surface modification. The current state of knowledge and progress in surface carbenes were comprehensively discussed in a recent review.[1−3] The following are just a few examples: insertion of adsorbed methylene, the simplest carbene, into metal-alkyl bonds on the surface was examined for how chain growth proceeds in Fischer−Tropsch synthesis.[4,5] Surface alkylidene monolayers were observed to be catalytically active in the heterogeneous version of the olefin metathesis reaction.[6−8] The anchoring of *N*-heterocyclic carbenes (NHCs) to planar gold surfaces was demonstrated to render surfaces accessible to further chemical derivatization,[9−11] for instance, through surface-initiated ring-opening metathesis polymerization.[11] Recently, an archetypal electrophilic aromatic carbene of extreme reactivity, fluorenylidene, was successfully generated and sharply imaged on a metal surface through high-resolution scanning tunneling microscopy.[12]

Ketocarbenes constitute another subclass of carbenes; however, in addition to some of the reactions that regular carbenes can participate in, including insertions into C−H bonds, additions to double bonds, and dimerization to form alkenes, ketocarbenes act as putative intermediates in Wolff rearrangement (WR), which is a 1,2-rearrangement reaction of

Received: October 18, 2021
Revised: January 19, 2022
Published: February 1, 2022

https://doi.org/10.1021/acs.jpcc.1c09050
J. Phys. Chem. C 2022, 126, 2482−2492

α-diazo carbonyl compounds accompanied by dinitrogen split-off, leading to ketene formation (Scheme 1).[13] WR can be

Scheme 1. Thermal, Photochemical, or Metal-Catalyzed Activation of α-Diazocarbonyl Compounds for Ketocarbene and Ketene Intermediate Production

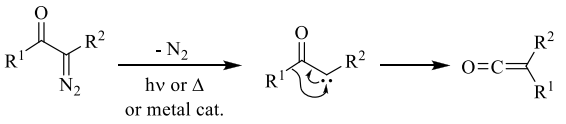

induced upon exposure to light or heat. Alternatively, transition-metal-catalyzed WR is also practiced, particularly over *silver* salts, but the mechanistic role of the metal remains unclear.[14] Whether WR involves a stepwise process with a carbene as an actual intermediate or is instead a concerted process leading directly from the excited state of the precursor to the ketene has also been debated. Among various types of diazo carbonyl molecules, diazoesters (R^1 = OR) are known not to undergo efficient WR rearrangement to provide ketenes because of the poor migratory aptitude of the −OR group; therefore, they decompose to form trappable ketocarbenes that may subsequently isomerize to ketenes (WR products) or be consumed in other decay routes. In fact, carbenes can engage in a self-coupling reaction to dimerize into alkenes (carbenic products). Although this path often seems to be an undesired side reaction, the dimers can actually be employed as a stable carbene reservoir that liberates reactive carbenes in situ. Furthermore, the simultaneous detection of carbene and its olefinic dimer can be viewed as unequivocal proof of a carbene, as described by the Wanzlick equilibrium.[15,16]

In the current study, preparation of an intercepting carboalkoxycarbene intermediate on a metal surface was attempted with adsorbed methyl diazoacetate (MDA, $N_2CHC(=O)OCH_3$, R^1 = OCH_3, R^2 = H), which served as the precursor. Because of its reluctance to 1,2-OR shift, MDA is more likely to take the carbene-mediated pathway and provide an opportunity for the desired carbene to be generated and interrogated. Unlike NHCs, the targeted carbene would be: $CHC(=O)OCH_3$ (carbomethoxycarbene or methyl ester-carbene), which lacks heteroatom stabilization and bulky shielding groups attached to the divalent carbon atom; therefore, it is inherently less stable and has been less investigated.[17−19] Silver was selected as the prime surface because Ag is known to accommodate carbenes.[12,20] The mode of carbene generation (thermal or photochemical) determines which spin state will be obtained; consequently, a quite different chemistry might be exhibited. The tamed surface carbenes are expected to retain some stability for characterization but to display reaction characteristics of the free species or divergent paths under the influence of the underlying silver surface. Here, we tested whether methyl ester-carbene can be stabilized on an Ag(111) surface and probed its postphotolysis chemistry using reflection−absorption infrared spectroscopy (RAIRS) and thermal desorption−mass spectrometry (TD−MS) complemented with density functional theory (DFT) calculations. Direct observation of methyl ester-carbene was achieved, and new insights into controlling the carbene reactivity and product selectivity by a metal surface were obtained.

METHODS

TD−MS and RAIRS Measurements. The experiments were performed under UHV conditions (<1.0×10^{-10} Torr). A clean, well-ordered Ag(111) surface was achieved by repeated cycles of Ar^+ sputtering and annealing at 950 K and judged to be free of impurities by Auger electron spectroscopy (AES). MDA and ethyl diazoacetate (EDA) were synthesized according to reported procedures by diazotization of glycine alkyl ester hydrochloride.[21]

Normal TD−MS measurements were performed by exposing the Ag(111) crystal to sample vapors at 100 K and then ramping the temperature to 950 K at a rate of 120 K/min. Upon heating, multiple ion signals and temperatures were collected synchronously. RAIRS was performed by exploiting the infrared beam from a Fourier transform infrared spectrometer. The beam penetrates and exits the UHV chamber through differentially pumped O-ring-sealed KBr windows and passes through a polarizer before entering the system. The IR source and detector used depend on the spectral region. Here, a liquid nitrogen-cooled HgCdTe detector was used in the 650−4000 cm^{-1} regime. Typical spectra were acquired as averages of 256 scans at a 4 cm^{-1} spectral resolution and normalized with respect to the background spectra from the clean metal surface. The optical path was purged with dry nitrogen gas to remove water vapor interference. Gas exposures are presented in units of langmuirs (1 langmuir = 1 L = 10^{-6} Torr s).

For photolysis, the sample was illuminated inside the UHV system by a light-emitting diode (LED) source that provided photons in the 365 ± 10 nm spectral region of the state. The LED head was mounted on a fused silica re-entrant viewport of the chamber to achieve a suitable focusing distance (38 mm), with an estimated photon peak intensity of ∼750 mW/cm^2. The light was directly shined through the window to give an irradiation spot with a diameter of ∼20 mm that covered the entire surface area. Postphotolysis TD spectra or mass responses as a function of irradiation time were collected by positioning the sample face 45° with respect to the light source and the quadrupole mass spectrometry (QMS) head at the specular reflection angle.

Computational. All DFT calculations were executed using the Gaussian 09 program package[22] at the B3LYP level of theory[23,24] with D3 dispersion corrections.[25] We employed the 6−31G(d) + LANL2DZ mixed basis set, which uses an ECP on the transition metal, and a Pople-type basis set on all other atoms. The Ag(111) surface was modeled by a two-layer Ag_{34} cluster, with 21 atoms in the first layer and 13 atoms in the second layer. Two sets of computational schemes were used. In the first set of calculations, which involved only molecular species such as MDA and dimethyl maleate (DMM), the Ag_{34} cluster was frozen with the Ag−Ag interatomic distances fixed at the bulk value (2.89 Å). In the second set of calculations regarding reactive intermediate species, six core Ag atoms of the top surface layer and one middle Ag atom of the second layer close to the adsorbate were allowed to relax during geometry optimization. All optimizations were performed with tight convergence criteria and an ultrafine integration grid. IR frequencies were calculated to confirm the nature of the stationary points and to obtain zero-point energies. The frequencies given were corrected using the recommended scaling factor of 0.96 to compensate for the absence of anharmonicity in these types of computations,[26] unless

https://doi.org/10.1021/acs.jpcc.1c09050
J. Phys. Chem. C 2022, 126, 2482−2492

otherwise stated. We used the GaussView visualization program to observe the normal modes for vibration assignments.

RESULTS

Control of MDA Surface Coverage. Optimizing the extent of grafting precursor molecules onto the surface is desirable for the subsequent generation and detection of carbenes. The effect of the MDA dose on its adsorption coverage at 100 K was probed through TD−MS and RAIRS. We used the parent ion with m/z 100 to track intact MDA molecular desorption in TD−MS measurements. Coverage-dependent TD spectra were taken at various exposures, including 1.0, 2.0, 3.0, 5.0, and 10.0 L, as shown in Figure 1a. At a 1.0 L exposure, a single desorption feature starts to emerge with a peak maximum at 210 K, which we associate with the molecular desorption of a monolayer. This desorption feature continues to grow until 3.0 L and saturates at 5.0 L. At coverages exceeding one monolayer (>5.0 L), one additional feature appears on the lower temperature side of the first peak and eventually develops into a second peak centered at 170 K, which we assigned to the MDA multilayers because this peak grows indefinitely in intensity with increasing exposure. The fact that desorption from monolayer MDA can be well resolved from multilayer MDA indicates that the bonding between MDA and the silver surface is slightly stronger than the intermolecular interactions of MDA molecules that occur within the condensed adlayers. Evidently, completion of a full monolayer should occur between 3.0 and 5.0 L. For follow-up experiments, a fixed exposure of 3.0 L (unless otherwise specified) was employed to achieve a balance between the coverage of reactants and the number of free sites. Coverage-dependent RAIR spectra are shown in Figure 1b. In contrast to the TD spectra, the IR absorption bands attributable to MDA only become observable above 2.0 L. A comparison of the spectra of the overlayer species (2.0 and 3.0 L) with those of the condensed multilayers (5.0 and 10.0 L) exhibits several differences, among which the most noticeable are the total and intensities of the various bands. At low coverages, oscillating dipoles parallel to the metal surface can be canceled by their image dipoles; therefore, only perpendicular modes are IR-active. At high coverages, image dipole effects are less pronounced, and the 100 K multilayer structure is likely to be disordered. The entire IR absorption bands and their intensities can be assigned to randomly oriented bulk molecules. Indeed, agreement between the IR bands in the multilayer spectrum (10.0 L MDA/Ag(111)) and those of neat MDA is excellent,[27] with signature bands at 2125 (C═N═N asymmetric stretching), 1692 (C═O stretching), 1445 (CH_3 deformation), 1382 (α-CH bending), 1211 ($(C-O)_{ester}$ stretching), and 1047 cm^{-1} ($(C-O)_{methoxy}$ stretching). However, because only peaks at 2125 and 1445 cm^{-1} exist in the overlayer regime, upon adsorption, the O−C(═O)−C plane of MDA molecules is perhaps nearly parallel to the Ag(111) surface—but with its O−CH_3 and N═N bonds tilted from horizontal (see Figure S1 in the Supporting Information for a minimum-energy structure of MDA bonded to the Ag_{34} surface model obtained by DFT geometry optimization).

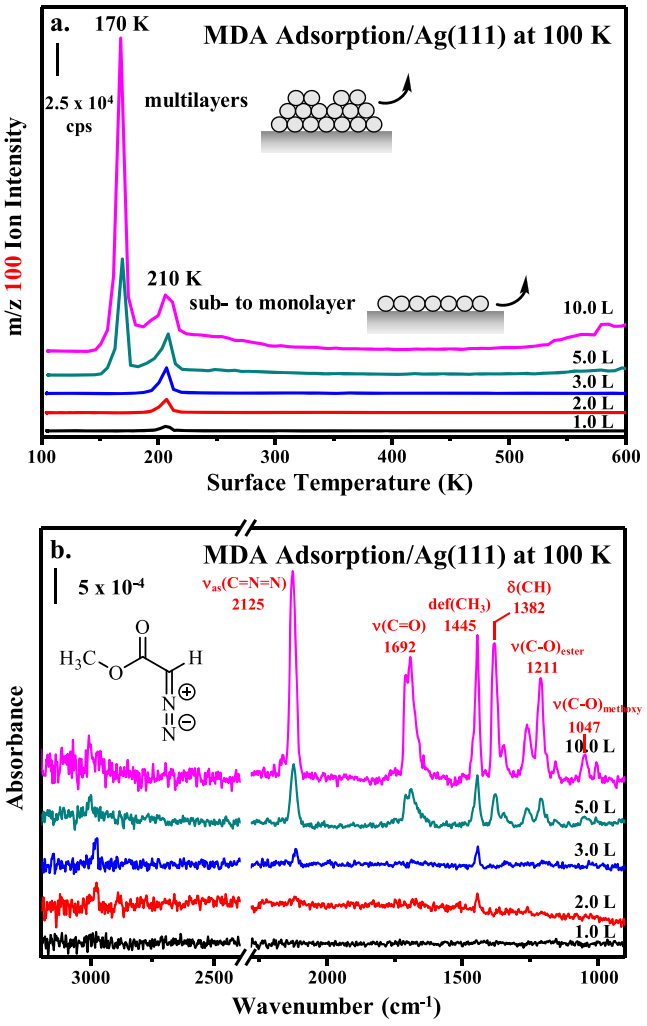

Figure 1. (a) Intact MDA (m/z 100) TD spectra from various exposures of MDA on Ag(111) at 100 K. (b) RAIR spectra with increasing exposures of MDA on Ag(111) at 100 K. The region between 2300 and 2400 cm^{-1}, which exhibits background CO_2 bands, has been omitted for clarity. (Symbols: cps = counts per second; ν_{as} = asymmetric stretching; ν = stretching; def = deformation; and δ = bending.)

Activation of Adsorbed MDA on Ag(111). We investigated treatment with heat and light to determine whether surface-bound MDA cleaves to yield the desired methyl ester-carbene and a free N_2 molecule. The thermolysis process was probed with a series of RAIR spectra obtained after annealing the adsorbed MDA to specific temperatures, as shown in Figure 2a. Annealing from 100 to 180 K led to increased peak sharpness and heights, indicating a reordered overlayer structure. Soon after annealing to temperatures above 200 K, all the bands in the RAIR spectra vanished, which coincides with the situation wherein MDA began to desorb molecularly. We conclude that the adsorbed MDA cannot be activated thermally on Ag(111).

At the beginning of the investigation of the photolysis of MDA, the UV−vis absorbance spectrum of MDA was analyzed (Figure S2). An absorption peak due to the $n-\pi^*$ transition of the diazo group[28] is observed at 380 nm; therefore, MDA was possibly activated by a high-intensity LED source, which may have provided photons in the wavelength region of 365 nm within a narrow spectral profile (~20 nm full width at half-maximum). A preannealing treatment at 180 K was conducted to remove extraneous adspecies from the background and to assemble the adsorbed MDA molecules into more well-ordered overlayer structures prior to light exposure. In stark contrast, a

https://doi.org/10.1021/acs.jpcc.1c09050
J. Phys. Chem. C 2022, 126, 2482−2492

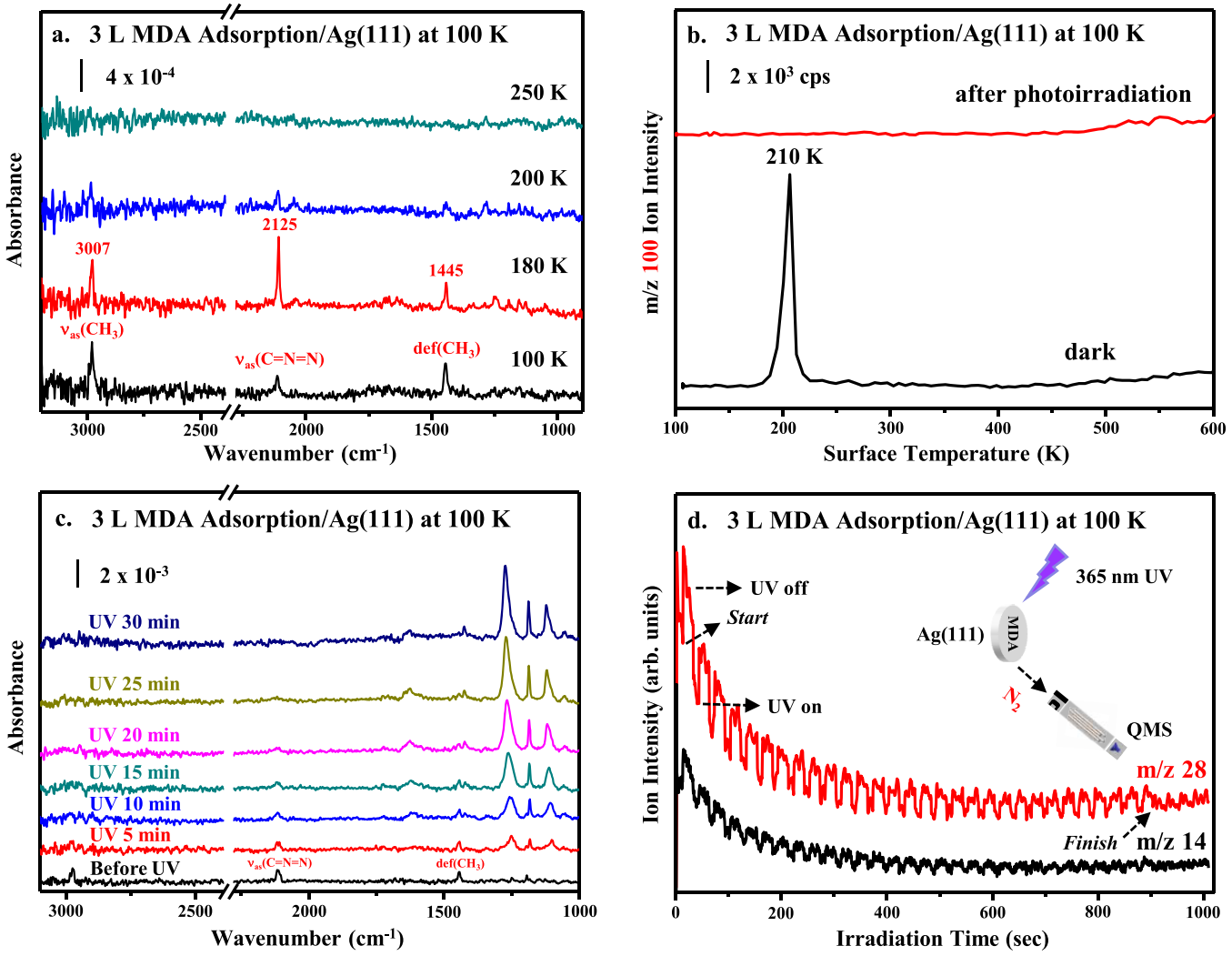

Figure 2. (a) RAIR spectra obtained following a 3.0 L MDA exposure at 100 K and, after annealing to the indicated temperatures, holding at those temperatures for 60 s, and then cooling back to 100 K, where the spectra were taken. (b) Comparison of TD spectra of intact MDA (m/z 100) with and without 365 nm UV photoirradiation (30 min) after dosing 3.0 L MDA onto Ag(111) at 100 K. (c) Trend of the RAIR spectra of the MDA overlayer recorded after exposure to 365-nm UV light for various times. (d) QMS responses of N_2 (m/z 28 and 14) ejection as a function of irradiation time obtained during the photolysis of the MDA overlayer at 365 nm (photon flux ~1.38×10^{19} photons/s·cm^2).

30 min exposure of MDA on the silver surface to 365 nm UV light at 100 K led to an entirely different outcome than that resulting from simple thermal annealing (in darkness). The intact molecular desorption feature at m/z 100 is completely absent from the postirradiation TD spectrum (see Figure 2b). In addition, the entire sequence of RAIR spectra (recorded every 5 min) underwent drastic changes during 30 min of UV illumination (see Figure 2c). Notably, the diagnostic C═N═N stretching mode of the precursor disappeared upon photoirradiation, indicative of the depletion of the diazo functionality of MDA. To identify the 365 nm light-induced ejection of the photolysis fragments in situ, the photon flux was alternately turned on and off as we followed the mass spectrometer responses as a function of time. Figure 2d shows the kinetic decay profiles upon the photoextrusion of nitrogen molecules, monitored using m/z 28 (N_2^+) and 14 (N^+) ion signals. The rise and fall pattern resonates with the switching between the "on" and "off" states of the LED source, which is strong proof of the loss of N_2 from adsorbed MDA during photolysis. All the mentioned results prompted speculation regarding whether we realized the capture of carbene intermediates after photolysis.

Evidence for Surface Ester-Carbene Following Photolysis of the Diazoester Precursor. Herein, we devised a potential route to stabilize methyl ester-carbene on an Ag(111) surface through photoextrusion of N_2 from MDA ($N_2CHC(═O)OCH_3$) at cryogenic temperatures. This approach enabled us to identify methyl ester-carbene by comparing the infrared spectra resulting from photolysis with the theoretical vibrational spectra calculated for the carbenic "$CHC(═O)OCH_3$" moiety anchored to a two-layer Ag_{34} cluster as the model surface (Figure 3). This cluster/adsorbate complex was geometrically optimized using a total energy minimization technique; its structure is illustrated and labeled 1-a in Scheme 2, which reveals that the methyl ester-carbene is coordinated to two Ag atoms to undergo 2-fold bridge-site bonding with Ag−C distances of 2.16 and 2.28 Å. The two Ag atoms to which carbene is connected are surrounded by other Ag atoms to ensure no edge effects. The C═O axis is slightly inclined and points down toward the underlying surface (~16°), while the O−CH_3 group is upright and extends into vacuum. The C═O

https://doi.org/10.1021/acs.jpcc.1c09050
J. Phys. Chem. C 2022, 126, 2482−2492

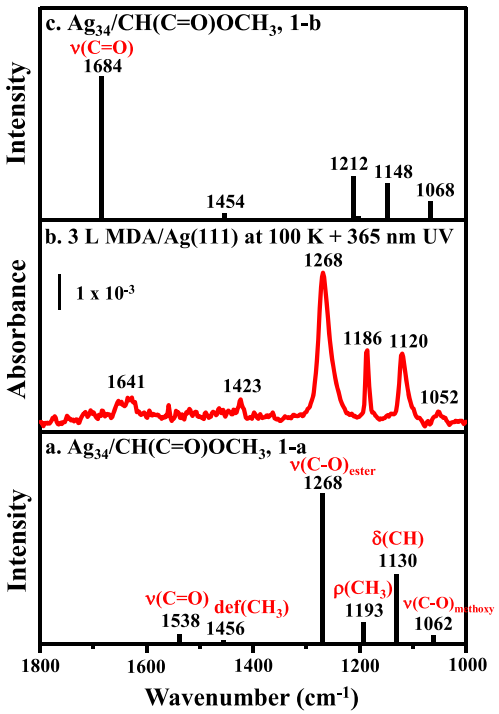

Figure 3. (a) Spectrum calculated from the DFT-optimized Ag_{34}/methyl ester-carbene structure with the oxygen atom of the *carbonyl* group bonded to a surface Ag atom (see Scheme 21-a). (b) Experimental RAIR spectrum of the MDA overlayer photolyzed by UV irradiation at 100 K. (c) Spectrum calculated from another Ag_{34}/methyl ester-carbene conformer with the oxygen atom of the *ester* group bonded to a surface Ag atom (see Scheme 21-b). The calculated vibrational frequencies are scaled by a factor of 0.98. (Symbols: ν = stretching; def = deformation; ρ = rocking; and δ = bending.)

Scheme 2. Optimized Structures of Two Methyl Ester-Carbene Conformers Coordinated to a Two-Layer Ag_{34} Cluster in DFT Calculations

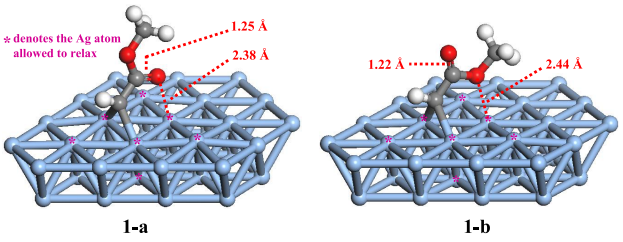

bond length of 1.25 Å is somewhat longer than that typical of a carbonyl double bond (1.23 Å). The O atom of the C═O group is in immediate contact with the surface Ag atom at a relatively short distance of 2.38 Å. An expanded view of the experimental spectrum (1000 to 1800 cm^{-1}) is juxtaposed with the simulated spectrum for close inspection in Figure 3b,a. The peak assignments in 3a are based upon animations of the computed normal modes, and the theoretical vibration frequencies are multiplied by a scaling factor of 0.98 to align the most intense predicted $(C-O)_{ester}$ stretching peak with the most intense experimentally measured band at 1268 cm^{-1}. It is intriguing that no intense peaks can be spotted in the carbonyl stretching region (between 1600 and 1800 cm^{-1}) in 3b. The weak feature predicted at 1538 cm^{-1} in 3a actually corresponds to C═O stretching, but with its dynamic dipole almost parallel to the supporting surface (see 1-a in Scheme 2); therefore, this mode is invisible in the experimental spectrum in 3b considering the surface dipole selection rule. The predicted redshift of this mode (from the typical ester carbonyl value of 1750 cm^{-1} to the current value of 1538 cm^{-1}) indicates a strong interaction with the metal support. The tiny feature at 1456 cm^{-1} in 3a ascribed to CH_3 deformation echoes the observed band at 1423 cm^{-1} in 3b. The two other pronounced bands at 1186 (terminal CH_3 rock) and 1120 cm^{-1} (α-CH bend) together with a weak mode at 1052 cm^{-1} ($(C-O)_{methoxy}$ stretching) observed in 3b match fairly well with the predicted frequencies—to less than 1%. The relative integrated peak intensity ratios of the three major experimental bands (1268, 1186, and 1120 cm^{-1}) are 100:15:33, which agree reasonably with the calculated peak height ratios of 100:14:46 considering the difficulty in computing accurate intensities at the harmonic level. Additionally, we notice a tiny broad absorption feature just barely above the noise level at approximately 1641 cm^{-1} in 3b, which fits with the frequency of the C═O stretching mode obtained from another Ag_{34}/CHC(═O)OCH_3 conformer (labeled 1-b in Scheme 2), where the orientation of the carbonyl group in the ester-carbene unit, after rotating around the C−C bond, becomes normal to the surface, rendering this vibration mode the strongest peak in the calculated spectrum at 1684 cm^{-1} (see Figure 3c). In this adopted configuration, the distance between the ester C−O oxygen atom and the nearest surface Ag atom is as close as 2.44 Å. However, geometry-optimized conformer 1-b has a slightly higher energy than conformer 1-a (by ∼3 kcal/mole), and the spectrum calculated for the less stable conformer, conformer 1-b, does not quite reproduce the observed spectrum regarding the entire peak pattern. Particularly, the extremely low intensity of the 1641 cm^{-1} band (not entirely indiscernible) in the experimental IR spectrum implies that conformer 1-b may not be forbidden but would be quite scarce. Overall, the data consistently suggest that photogenerated methyl ester-carbene species did not elude us, and we succeeded in their isolation and spectroscopic characterization on Ag(111) at low temperature.

Postphotolysis Chemistry: Stereoselective Ester-Carbene Dimerization. After confirmation of it being the primary photoproduct, methyl ester-carbene underwent substantial alteration when its surface was annealed from 100 to 200 K, and pronounced changes in the RAIR spectra occurred (Figure 4a−c). In particular, the decay of four major carbenic bands at 1268, 1186, 1120, and 1052 cm^{-1} is concomitant with the emergence of new features at 2033, 1700, 1584, 1281 (unresolved), 1195, 1126, and 1064 cm^{-1} in the 160 K spectrum, suggesting the formation of one or more new chemically distinct intermediates. The latter set of peaks continues to increase in magnitude and reaches a maximum after annealing to 200 K. Based on carbene chemistry, we are able to narrow the possible candidates to a handful, such as DMM and dimethyl fumarate (DMF) (*cis* and *trans* olefins from methyl ester-carbene dimerization) as well as methoxyketene (a WR product from the 1,2-OCH_3 shift of methyl ester-carbene in Scheme 1). To gauge the spectral similarity, we measured the RAIR spectra for the authentic samples on Ag(111). The data in Figure 4d,e demonstrate that the spectra of DMM, (*cis*-alkene) and DMF (*trans*-alkene) are sufficiently different to allow the two stereoisomers to be distinguished on the surface. The outstanding feature at 1000 cm^{-1} shown in Figure 4e is particularly diagnostic of DMF. The lack of this

https://doi.org/10.1021/acs.jpcc.1c09050
J. Phys. Chem. C 2022, 126, 2482−2492

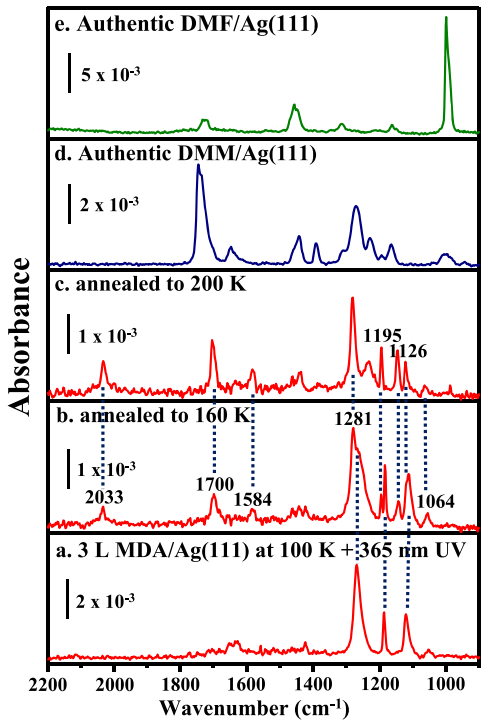

Figure 4. (a) Experimental RAIR spectrum of surface-bound methyl ester-carbene generated by MDA photolysis. (b,c) Postphotolysis RAIR spectra obtained after annealing (a) to the indicated temperatures. (d,e) RAIR spectra of authentic samples of methyl ester-carbene dimers: DMM (*cis*-dimer) and DMF (*trans*-dimer).

band in Figure 4c can thus exclude DMF from the product list. Indeed, except for the peaks at 2033 and 1064 cm^{-1}, the remainder of the experimental spectrum (4c) can be assigned solely to DMM. Hence, the selectivity approaches 100%. DFT geometry optimization creates a minimum-energy structure of DMM bonded to the Ag_{34} surface model. The resulting calculated vibration frequencies, along with their mode assignments, can also nearly replicate the IR peaks in the corresponding experimental spectrum (Figure S3 and Table S1). To substantiate the stereoselective identification, characteristic mass fragmentation patterns of authentic DMM and DMF were also obtained using a mass spectrometer (70 eV EI); they are demonstrated in two separate panels in the insets of Figure 5. Enediester compounds usually have an extremely weak or nonexistent parent ion peak (M^+, m/z 144) but often lose one OR (R = CH_3) group to demonstrate a strong peak of $(M-31)^+$ at m/z 113. Further C═O elimination affording an m/z 85 ion ($(M-31-28)^+$) is also common, and esters always have a fragment because of $C(=O)OR^+$ (R = CH_3, m/z 59). Notably, the ratio of the relative abundances of m/z 113, 85, and 59 ions for DMM is 100:35:30, distinguishable from that (100:100:44) for DMF. Postphotoirradiation TD measurements of Ag(111) exposed to 3.0 L MDA at 100 K were performed to detect the evolution of gaseous DMM and/or DMF. In Figure 5a, the resulting TD spectra exhibit a major desorption state that encompasses a set of concurrent m/z 113, 85, and 59 profiles centered at approximately 250 K with relative integrated peak intensity ratios of 100:40:38, consistent with the values of DMM. Clues supporting stereoselective formation of maleate over fumarate in ester-carbene dimerization were thus established. To prove that only the *cis* carbene dimer forms, we examined the same chemistry

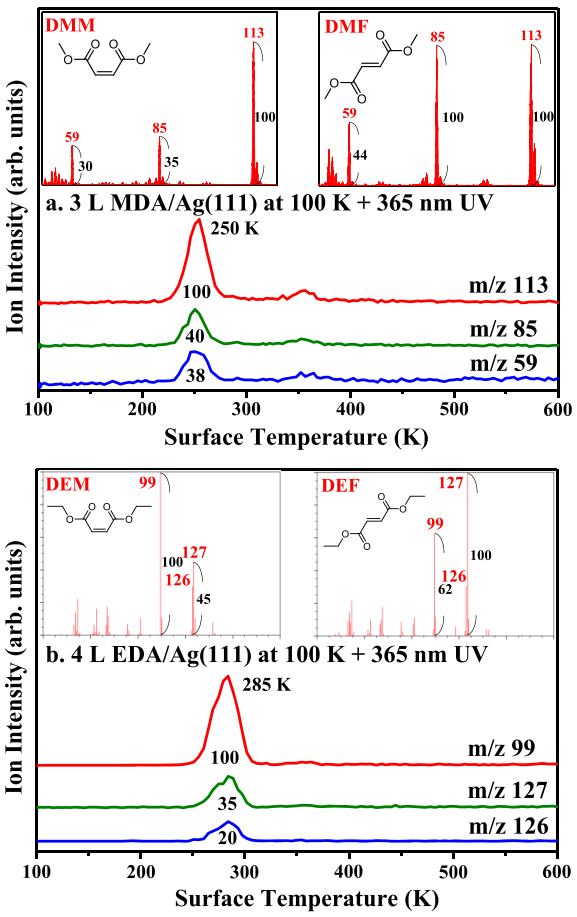

Figure 5. (a) Multiple-ion TD spectra obtained from the MDA overlayer subjected to sufficient 365 nm UV irradiation exposure. Major ion fragments of the carbene dimers (m/z 113, 85, and 59) were monitored. Insets are mass fragmentation patterns measured for authentic DMM and DMF in an ultrahigh vacuum chamber at a 1.0×10^{-8} Torr vapor pressure. (b) Same type of measurement for EDA. The corresponding carbene dimers, DEM and DEF, are represented by peaks at m/z 99, 126, and 127. Insets are fragmentation patterns of DEM and DEF documented in the NIST database.[29]

from the ethoxy-substituted version. As shown in the insets of Figure 5b, the differences between the mass fragmentation patterns of diethyl fumarate (DEF) and diethyl maleate (DEM) are even more drastic (documented in the NIST Chemistry WebBook),[29] where the most abundant ion in the reference DEF is the m/z 127 ion ($(M-OC_2H_5)^+$, i.e., $(M-45)^+$), whereas the strongest peak in DEM is at m/z 99 ($(M-45-28)^+$) following an additional loss of CO. In practice, EDA ($N_2CHC(=O)OC_2H_5$), an ethyl ester-carbene precursor, was dosed onto Ag(111) followed by sufficient exposure to 365 nm light at 100 K, and the postirradiation TD spectra, with the m/z 99 fragment ion being dominant, indeed provide evidence of the exclusive formation of DEM as the *cis*-selective carbene dimer (Figure 5b).

Surface-Mediated C–O Bond Cleavage of Methyl Ester-Carbene. Apart from those assigned to DMM, the IR bands at 2033 and 1064 cm^{-1} in the 200 K spectrum (Figure 4c) indicate a different fate of methyl ester-carbenes in addition to dimerization. WR of MDA, with the migration of $-OCH_3$ to form methoxyketene ($O=C=CH(OCH_3)$), was expected to be inefficient (heteroatoms have a low propensity to shift positions). Furthermore, according to a study regarding

https://doi.org/10.1021/acs.jpcc.1c09050
J. Phys. Chem. C 2022, 126, 2482−2492

a ketene monolayer on a Pt single-crystal surface,[30] the characteristic vibration frequency of ketene species corresponding to C═C═O asymmetric stretching is approximately 30 cm^{-1} higher than that corresponding to C═N═N asymmetric stretching (2125 cm^{-1} for MDA). Here, the band at 2033 cm^{-1} is too low in frequency to be assigned to methoxyketene, and the lack of ketene thus precludes the possibility of a WR pathway. Instead, a precedent for the metal-catalyzed activation of acyl C−O bonds in methyl esters via a three-centered transition state exists;[31] therefore, we speculate that this 2033 cm^{-1} band originates from a surface ketenyl group (CH═C═O) that calls for facile conversion of methyl ester-carbene conformer 1-a to 1-b (recall Scheme 2), which has an ester C−O bond in the correct orientation, with the oxygen atom directed toward the metal surface, and is thus amenable to C−O bond cleavage, namely, Ag/CHC(═O)−OCH_3 (1-b) → Ag/CH═C═O + Ag−OCH_3. The ketenyl group might even undergo rapid, reversible H-transfer of α-CH to a pair of silver surface-bound ketenyl and ketenylidene/hydride tautomers, that is, $CH{=}C{=}O_{(ad)} \rightleftarrows C{=}C{=}O_{(ad)} + H_{(ad)}$.[32] Further verification can be gained through excellent agreement between the 200 K experimental spectrum (Figure 6a, where DMM is labeled with asterisks) and a combination

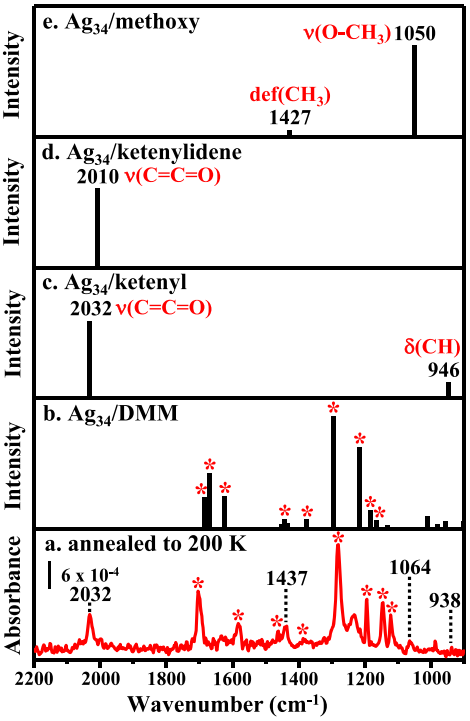

Figure 6. (a) Postphotolysis RAIR spectrum after thermal annealing at 200 K, at which several chemically distinct intermediates might form. Possible IR bands of DMM are labeled with asterisks. (b−e) Calculated spectra of speculated surface species, including Ag_{34} cluster-bound DMM, CH═C═O, C═C═O, and OCH_3 (see Scheme 3 for their DFT-optimized structures).

of computed spectra for all the hypothesized intermediate species, including DMM, ketenyl (2032 cm^{-1}, C═C═O stretching), ketenylidene (2010 cm^{-1}, C═C═O stretching), and methoxy (1050 cm^{-1}, O−CH_3 stretching) bonded to the Ag_{34} cluster (see Scheme 3 for structures 2, 3, 4, and 5), as shown in Figure 6b−e. The reported diagnostic vibrational frequencies of Ag(111)-bound methoxy at 1048 cm^{-1} (O−CH_3 stretching)[33] and ketenylidene at 2026 cm^{-1} (asymmetric C═C═O stretching)[34] are also in accordance with our identification.

Scheme 3. DFT-Optimized Structures of a Single DMM, Ketenyl, Ketenylidene, and Methoxy Unit Bound to the Ag(111) Surface of an Ag_{34} Cluster Model

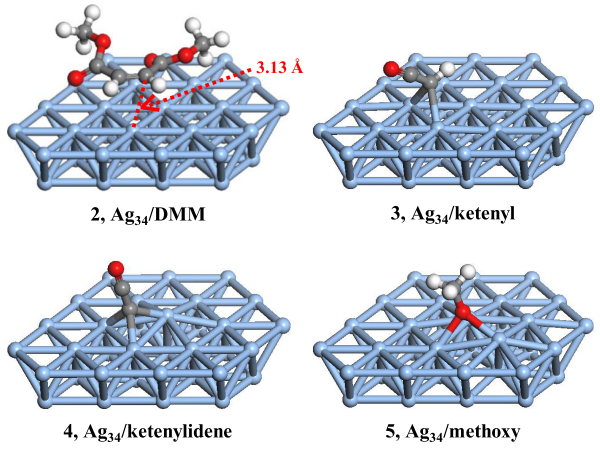

Subtle Spectral Changes from 200 to 300 K: Side-on η^2(CO) Adsorption Mode of DMM. Further annealing to 300 K engendered slight variations in the RAIR spectrum (Figure 7). The intensity of the peak at 1569 cm^{-1} (C═C

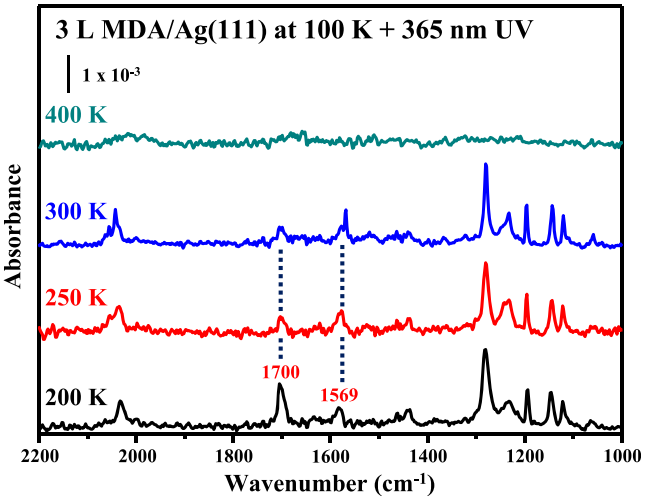

Figure 7. Series of postphotolysis RAIR spectra measured after annealing to the indicated temperatures.

stretching of DMM) increases at the expense of a decrease in the peak at 1700 cm^{-1} (C═O stretching of DMM). Schröder et al. worked on the surface assemblies of ethyl pyruvate (EP) and reported an IR band at 1530 cm^{-1}, which they assigned to a side-on η^2(CO) adsorption configuration of the ester-carbonyl group, rather than C═C in the enol form of EP.[35] Because of pronounced mixing of the carbonyl orbitals with those of underlying surface metal atoms, the $(C{=}O)_{ester}$ stretching vibration frequency can be substantially shifted from its unperturbed value (~1750 cm^{-1}) to 1520−1585 cm^{-1}. Inspired by this information, we attribute the temperature-dependent trade-off between the 1700 and 1569 cm^{-1} peak intensities to the increased population of side-on coordinated DMM. Uncoincidentally, the partial molecular

https://doi.org/10.1021/acs.jpcc.1c09050
J. Phys. Chem. C 2022, 126, 2482−2492

desorption of DMM from a crowded surface occurred at 250 K (see Figure 5a), presumably leaving more adsorption sites open. Hence, the remaining surface DMM molecules were prone to the flat-lying η^2(CO) bonding mode.

The RAIR spectrum taken after annealing to 400 K (Figure 7) is not described. Increasing the temperature to 400 K must readily trigger successive reactions to dispose of the vibration features of the entire spectrum. Such development in the RAIR spectrum mirrors the TD results shown in Figure 8.

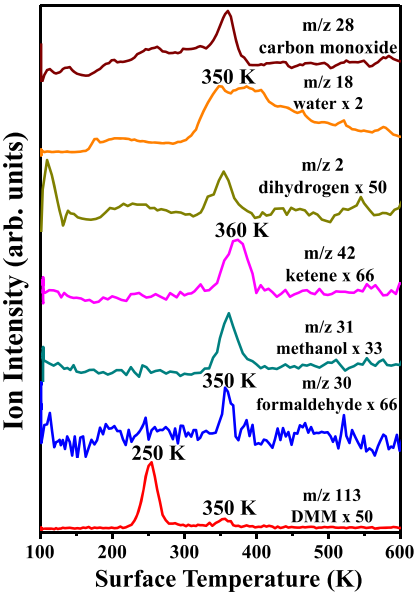

Figure 8. TD spectra of a variety of gas-phase products collected after adsorption of 3.0 L MDA on Ag(111) at 100 K followed by 180 K preannealing and photoextrusion of N_2 using 365 nm UV light at 100 K.

Survey of Final Gas-Phase Products by TD–MS. We determined the chemistry responsible for the disappearance of all IR bands above 300 K. Between 200 and 300 K, the surface adlayer exhibited notable DMM, ketenyl, ketenylidene/hydride, and (likely) methoxy species coverage. As shown in Figure 8, TD measurements indicated that the desorption of DMM (represented by m/z 113) proceeded in two steps—at 250 and 350 K. The methoxy group was stable at 300 K, above which methanol (m/z 31) and formaldehyde (m/z 30) desorbed simultaneously at 350 K, a process postulated to occur through the disproportionation of coadsorbed methoxy moieties. Alternatively, methoxy might undergo hydrogen abstraction by the metal surface to furnish formaldehyde and H atoms: $CH_3O_{(ad)} \rightarrow H_2CO_{(g)} + H_{(ad)}$. Interconversion between ketenyl and ketenylidene also produced H atoms during the exchange. Background hydrogen, which is invariably present in even the optimal ultrahigh vacuum environment, can create H atoms at the hot filament of the ion gauge. As a result, ketene (m/z 42), methanol (m/z 31), and H_2 (m/z 2) were found to evolve at approximately 350 K through the recombination of surface fragments: $CH{=}C{=}O_{(ad)} + H_{(ad)} \rightarrow CH_2 = C{=}O_{(g)}$, $CH_3O_{(ad)} + H_{(ad)} \rightarrow CH_3OH_{(g)}$, and $H_{(ad)} + H_{(ad)} \rightarrow H_{2(g)}$. On the clean Ag surface, methanol, H_2, and formaldehyde desorb below 230 K.[36−38] In this case, the fact that all products desorb together at approximately 350 K, well above their natural desorption temperatures, obviously indicates that the process is reaction-limited. Further C−O bond and C−H bond scissions in methanol and formaldehyde led to intense H_2O and CO desorption features. Species that were searched for but not found include methoxyketene (WR product), dimethyl acetylenedicarboxylate (DMAD, dehydrogenation product of DMM), and dimethyl succinate (hydrogenation product of DMM). We used AES to determine whether any residual surface species were present. No obvious traces of impurities, such as carbon (272 eV), nitrogen (379 eV), or oxygen (503 eV), were observed (Figure S4).

DISCUSSION

Proposed Mechanism. Based on available experimental and computational evidence, Scheme 4 is presented to reflect the photolysis and postphotolysis thermal chemistry: UV photodissociation involves an electronic transition that severs the bond between the diazo group and the carbon atom in the adsorbed MDA at 100 K, resulting in a species identified as methyl ester-carbene. Geometry optimization using DFT shows that two carbene conformers, 1-a and 1-b, exist as true energy-minimum structures with either the oxygen atom of the carbonyl or methoxy groups attached to the surface Ag atoms and that 1-a is more stable than 1-b. The RAIR spectrum (Figure 3b) can be interpreted accordingly, as carbenes 1-a and 1-b form an equilibrium mixture, with the

Scheme 4. Proposed Reaction Pathways Initiated by MDA Overlayer Adsorption on Ag(111)

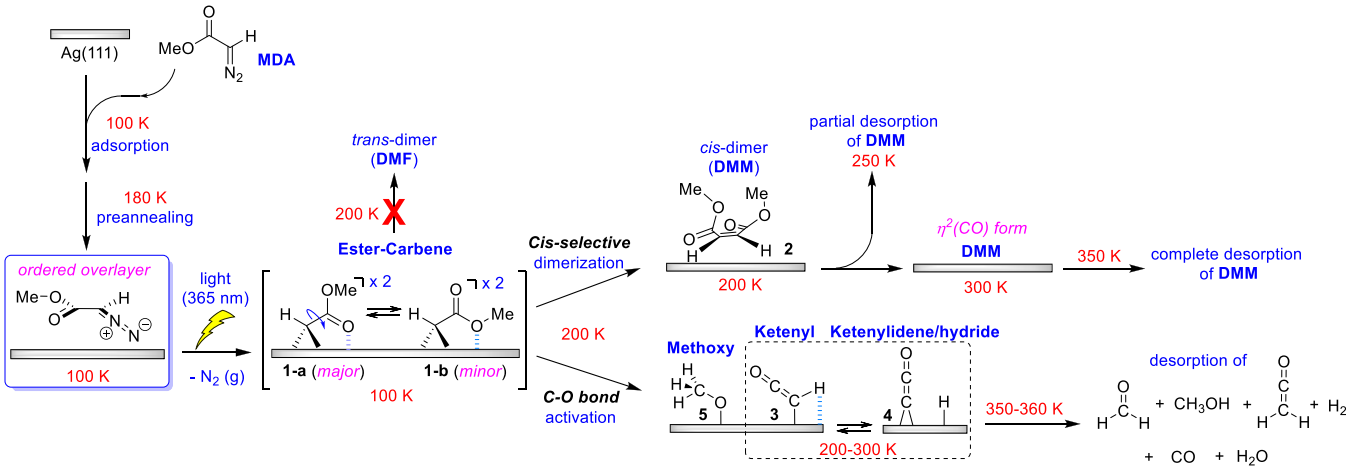

https://doi.org/10.1021/acs.jpcc.1c09050
J. Phys. Chem. C 2022, 126, 2482−2492

former being the dominant species. Postirradiation heating generates DMM (**2**, *cis*-form dimer), free of DMF (*trans*-form dimer) at 200 K, based on the RAIRS and mass spectral data (Figures 4 and 5). DMM sequentially desorbs intact from Ag(111) above 250 K. Part of the carbenic species undergoes selective ester C−O bond activation at 200 K to give surface-bound methoxy **5** along with a set of ketenyl **3** and ketenylidene/hydride **4** tautomers (200−300 K). Above 300 K, a variety of smaller species are generated, such as methanol and formaldehyde, which might form via the H-abstraction and/or disproportionation of methoxy group **5**. Ketenyl hydrogenates to ketene, and H atoms recombine to form H_2. Further decomposition of the organic species releases H_2O and CO.

Electron-Rich Carbenes. Natural population analysis (as implemented in the Gaussian 09 code) was performed to obtain greater insight into the nature of the metal−ligand bond. In our Ag_{34}/CHC(=O)OCH_3 calculations, the atomic charges on the carbene carbon are −0.866 and −0.860 for conformers 1-a and 1-b, respectively (Scheme 5). In either case, there is a net transfer of $0.68e^-$ or $0.59e^-$ from the underlying Ag framework to the adsorbed methyl ester-carbene. These results are admirably consistent with the reported DFT predictions of ethyl ester-carbene bound to an Au_{10} model meant to mimic gold nanoparticles.[18] The authors claimed that the electron-rich carbene was a consequence of charge transfer from the low-coordinated Au corner atoms to the antibonding orbitals of the ester C=O. In our cluster model, the top layer, containing 21 Ag atoms, has a sufficiently large area to minimize edge effects. Therefore, this trend of significant negative charges on the carbene carbon should be translated to extended planar surfaces. The strong anionic characters suggest that when the electron-rich carbenes are in close proximity, presumably the resulting repulsive electrostatic interactions would have a large destabilizing effect. To alleviate this, the carbene units facilely dimerize at 200 K.

Scheme 5. Charge Distributions of Two Ag_{34}/Methyl Ester-Carbene Conformers Evaluated by Natural Population Analysis

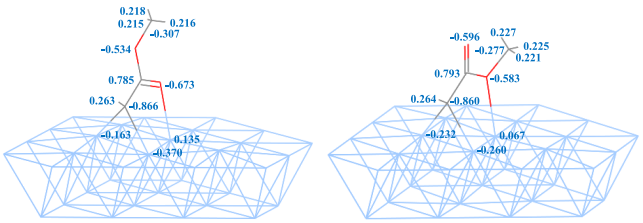

1-a 1-b

***Cis*-Selectivity.** Catalytic access to thermodynamically less stable *cis*-alkenes has received considerable attention.[39] The ability of the Ag surface to render homocoupling of ester-carbenes into exclusive *cis*-enediesters (maleates) is intriguing. Tysoe et al., in a study on the dimerization of ethylidene to *trans*-2-butene on Ag(111),[20] remarked that the stereoselectivity is controlled either by the ease of the initial approach of the two carbenes or by the stability of the *cis*- or *trans*-form intermediate. In this case, we suggest a rationale for the observed *cis*-selectivity by invoking the metallacyclic intermediacy in Scheme 6: we assume that the orderly arranged MDA adlayer enables the adjacent photogenerated ester-carbene species to be aligned parallel to each other, as shown in the left, facilitating orbital overlap between two carbenic carbon centers. The steric repulsion between the fairly large methyl ester groups of the approaching ester-carbenes disfavors the formation of a *cis*-intermediate, thereby making this initial step slow relative to that of its *trans*-form counterpart. However, the conjectured four-membered *trans* metallacyclic intermediate may be too stable due, particularly, to the significant interaction between the oxygen atoms and the underlying surface, which deters the subsequent formation of the corresponding *trans*-enediester compound (DMF). In stark contrast, the *cis* metallacycle is sterically congested and more strained; therefore, its unstable and transient nature moves the reaction rapidly forward to *cis*-enediester (DMM). Because of the fast removal of unstable *cis*-intermediates, the system responds by favoring a reaction that can continuously replace that substance. As a result, DMM prevails as the final product.

CONCLUSIONS

The interactions between Ag(111) and ester-carbenes appear to be sufficient to allow the target carbenes to be tamed at 100 K. As a result, methyl ester-carbene, stemming from the photoexcitation of MDA, is trapped and unambiguously characterized by three distinctive IR-active modes: ester C−O stretching, CH_3 rocking, and α-CH bending vibrations. Curiously, the more representative C=O feature is missing. The DFT-based theoretical framework explains that the

Scheme 6. Speculative Origin of *Cis*-Stereoselectivity Concerning Methyl Ester-Carbene Dimerization on Ag(111)

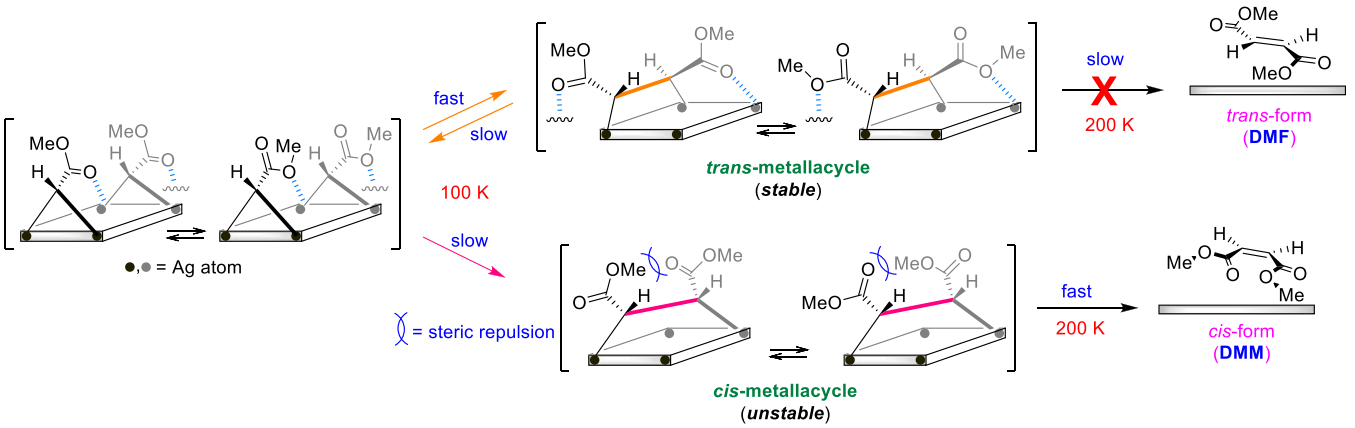

https://doi.org/10.1021/acs.jpcc.1c09050
J. Phys. Chem. C 2022, 126, 2482−2492

carbene carbon binds to two substrate Ag atoms and that further stabilization is achieved through the coordination of the oxygen atom of the C═O group to the Ag surface. The anticipated strongly redshifted C═O stretching vibration proves to be IR-forbidden by the surface dipole selection rule. The similarity between ester-carbene bound to Au nanoparticles[18] and an Ag surface supports electron back donation from the metal surface to the antibonding orbitals of the carbonyl group to render an electron-rich carbene. The resulting partially negative charges centered on the carbene carbon atoms are a driving force for the carbon−carbon bond formed between the two adjacent ester-carbenes, which reduces the electrostatic repulsions. Ester-carbenes can readily undergo a diagnostic carbene dimerization reaction at 200 K to discriminately form the *cis*-alkene end-product. Although forming the *trans*-intermediate seems to avoid steric hindrance between the approaching ester groups, the strict stereochemistry observed is presumably dictated by the relative stability of the two proposed differently aligned Ag−C−C−Ag metallacycles. The intensive interactions between the C═O (and/or C−O) groups and the metal surface bestowed upon the *trans*-metallacyclic intermediate have an adverse impact on its passage to the *trans*-isomer; therefore, the fate of the reaction is inclined toward the *cis*-isomer.

The ability to adjust surface properties through chemical modification of the monolayer is required in many applications. The incorporation of carbenes of high reactivity onto metal surfaces broadens the scope for adding functionality to a surface. In our study, ester-carbenes were proven to be electron-rich ligands on silver surfaces that, in principle, can react with electron-seeking reagents to achieve further chemical derivatization of the surface. Understanding the influence of surface attachment on carbene reactivity could lead to the development of new functional materials.

■ ASSOCIATED CONTENT

Supporting Information

The Supporting Information is available free of charge at https://pubs.acs.org/doi/10.1021/acs.jpcc.1c09050.

Additional calculated IR spectra, UV−vis absorption spectra, Auger electron spectra, and assignments of the vibrational modes of DMM (PDF)

■ AUTHOR INFORMATION

Corresponding Authors

Chi-Wi Ong − *Department of Chemistry, National Sun Yat-Sen University, Kaohsiung 80424, Taiwan*; Email: cong@mail.nsysu.edu.tw

Chao-Ming Chiang − *Department of Chemistry, National Sun Yat-Sen University, Kaohsiung 80424, Taiwan*; orcid.org/0000-0002-5021-9612; Email: cmc@mail.nsysu.edu.tw

Authors

Chia-Hung Wu − *Department of Chemistry, National Sun Yat-Sen University, Kaohsiung 80424, Taiwan*

Jean-Ho Chu − *Department of Applied Science, National Taitung University, Taitung 95092, Taiwan*; orcid.org/0000-0003-3366-2126

Chih-Hung Chou − *Department of Chemistry, National Sun Yat-Sen University, Kaohsiung 80424, Taiwan*

Po-Chiao Lin − *Department of Chemistry, National Sun Yat-Sen University, Kaohsiung 80424, Taiwan*

Complete contact information is available at: https://pubs.acs.org/10.1021/acs.jpcc.1c09050

Notes

The authors declare no competing financial interest.

■ ACKNOWLEDGMENTS

We thank the Ministry of Science and Technology, Taiwan, Republic of China, for funding under Grant Nos. MOST107-2113-M-110-006, MOST108-2113-M-110-009, and MOST109-2113-M-110-012.

■ REFERENCES

(1) Zhukhovitskiy, A. V.; MacLeod, M. J.; Johnson, J. A. Carbene Ligands in Surface Chemistry: From Stabilization of Discrete Elemental Allotropes to Modification of Nanoscale and Bulk Substrates. *Chem. Rev.* **2015**, *115*, 11503−11532.

(2) Engel, S.; Fritz, E.-C.; Ravoo, B. J. New Trends in the Functionalization of Metallic Gold: from Organosulfur Ligands to N-Heterocyclic Carbenes. *Chem. Soc. Rev.* **2017**, *46*, 2057−2075.

(3) Smith, C. A.; Narouz, M. R.; Lummis, P. A.; Singh, I.; Nazemi, A.; Li, C.-H.; Crudden, C. M. *N*-Heterocyclic Carbenes in Materials Chemistry. *Chem. Rev.* **2019**, *119*, 4986−5056.

(4) Wu, H.-J.; Chiang, C.-M. Distinct Demonstration of Methylene Insertion into the Metal-Carbon Bond on Ag(111). *J. Phys. Chem. B* **1998**, *102*, 7075−7077.

(5) Wu, H.-J.; Hsu, H.-K.; Chiang, C.-M. Surface Reactions of CH_3I and CF_3I with Coadsorbed CH_2I_2 on Ag(111) as Mechanistic Probes for Carbon-Carbon Bond Formation via Methylene Insertion. *J. Am. Chem. Soc.* **1999**, *121*, 4433−4442.

(6) Zahidi, E. M.; Oudghiri-Hassani, H.; McBreen, P. H. Formation of Thermally Stable Alkylidene Layers on a Catalytically Active Surface. *Nature* **2001**, *409*, 1023−1026.

(7) Siaj, M.; Reed, C.; Oyama, S. T.; Scott, S. L.; McBreen, P. H. Dissociation of Acetaldehyde on β-Mo_2C to Yield Ethylidene and Oxo Surface Groups: A Possible Pathway for Active Site Formation in Heterogeneous Olefin Metathesis. *J. Am. Chem. Soc.* **2004**, *126*, 9514−9515.

(8) Tulevski, G. S.; Myers, M. B.; Hybertsen, M. S.; Steigerwald, M. L.; Nuckolls, C. Formation of Catalytic Metal-Molecule Contacts. *Science* **2005**, *309*, 591−594.

(9) Crudden, C. M.; Horton, J. H.; Ebralidze, I. I.; Zenkina, O. V.; McLean, A. B.; Drevniok, B.; She, Z.; Kraatz, H.-B.; Mosey, N. J.; Seki, T.; et al. Ultra Stable Self-Assembled Monolayers of N-Heterocyclic Carbenes on Gold. *Nat. Chem.* **2014**, *6*, 409−414.

(10) Crudden, C. M.; Horton, J. H.; Narouz, M. R.; Li, Z.; Smith, C. A.; Munro, K.; Baddeley, C. J.; Larrea, C. R.; Drevniok, B.; Thanabalasingam, B.; et al. Simple Direct Formation of Self-Assembled N-Heterocyclic Carbene Monolayers on Gold and Their Application in Biosensing. *Nat. Commun.* **2016**, *7*, 12654.

(11) Zhukhovitskiy, A. V.; Mavros, M. G.; Van Voorhis, T.; Johnson, J. A. Addressable Carbene Anchors for Gold Surfaces. *J. Am. Chem. Soc.* **2013**, *135*, 7418−7421.

(12) Mieres-Perez, J.; Luchat, K.; Trosien, I.; Sander, W.; Sanchez-Garcia, E.; Morgenstern, K. Controlling Reactivity−Real-Space Imaging of a Surface Metal Carbene. *J. Am. Chem. Soc.* **2021**, *143*, 4653−4660.

(13) Wolff, L. Ueber Diazoanhydride. *Justus Liebigs Ann. Chem.* **1902**, *325*, 129−195.

(14) Sudrik, S. G.; Sharma, J.; Chavan, V. B.; Chaki, N. K.; Sonawane, H. R.; Vijayamohanan, K. P. Wolff Rearrangement of α-Diazoketones Using in Situ Generated Silver Nanoclusters as Electron Mediators. *Org. Lett.* **2006**, *8*, 1089−1092.

(15) Wanzlick, H. W. Aspects of Nucleophilic Carbene Chemistry. *Angew. Chem., Int. Ed. Engl.* **1962**, *1*, 75−80.

(16) Weidner, T.; Baio, J. E.; Mundstock, A.; Grosse, C.; Karthäuser, S.; Bruhn, C.; Siemeling, U. NHC-Based Self-Assembled Monolayers on Solid Gold Substrates. *Aust. J. Chem.* **2011**, *64*, 1177−1179.

(17) Ulman, M.; Belderrain, T. R.; Grubbs, R. H. A Series of Ruthenium(II) Ester-Carbene Complexes as Olefin Metathesis Initiators: Metathesis of Acrylates. *Tetrahedron Lett.* **2000**, *41*, 4689−4693.
(18) Oliver-Meseguer, J.; Boronat, M.; Vidal-Moya, A.; Concepción, P.; Rivero-Crespo, M. A.; Leyva-Pérez, A.; Corma, A. Generation and Reactivity of Electron-Rich Carbenes on the Surface of Catalytic Gold Nanoparticles. *J. Am. Chem. Soc.* **2018**, *140*, 3215−3218.
(19) Bai, D.; Jennings, G. K. Surface-Catalyzed Growth of Polymethylene-Rich Copolymer Films on Gold. *J. Am. Chem. Soc.* **2005**, *127*, 3048−3056.
(20) Wu, G.; Stacchiola, D.; Kaltchev, M.; Tysoe, W. T. A Study of the Stereoselectivity in the Dimerization of Ethylidene to Form 2-Butene on Ag(111). *J. Am. Chem. Soc.* **2000**, *122*, 8232−8237.
(21) Lam, J.; Johnson, B. Reaction of Norbornadiene with Methyl Diazoacetate. *Aust. J. Chem.* **1972**, *25*, 2269−2273.
(22) Frisch, M. J.; Trucks, G. W.; Schlegel, H. B.; Scuseria, G. E.; Robb, M. A.; Cheeseman, J. R.; Scalmani, G.; Barone, V.; Menucci, B.; Petersson, G. A. et al. *Gaussian 09, Revision C.01*; Gaussian, Inc.: Wallingford, CT, 2010.
(23) Becke, A. D. A New Mixing of Hartree-Fock and Local Density-Functional Theories. *J. Chem. Phys.* **1993**, *98*, 1372−1377.
(24) Lee, C. T.; Yang, W. T.; Parr, R. G. Development of the Colle-Salvetti Correlation Energy Formula into a Functional of the Electron Density. *Phys. Rev. B* **1988**, *37*, 785−789.
(25) Grimme, S.; Ehrlich, S.; Goerigk, L. Effect of the Damping Function in Dispersion Corrected Density Functional Theory. *J. Comput. Chem.* **2011**, *32*, 1456−1465.
(26) Merrick, J. P.; Moran, D.; Radom, L. An Evaluation of Harmonic Vibrational Frequency Scale Factors. *J. Phys. Chem. A* **2007**, *111*, 11683−11700.
(27) Leung-Toung, R.; Wentrup, C. Flash Vacuum Pyrolysis of tert-Butyl β-Ketoesters: Sterically Protected α-Oxoketenes. *Tetrahedron* **1992**, *48*, 7641−7654.
(28) Li, Y.-Z.; Schuster, G. B. Wavelength-Dependent Photochemistry of a Diazo Compound: Irradiation of 9-Diazo-1,8-diazafluorene with Ultraviolet or Visible Light. *J. Org. Chem.* **1987**, *52*, 4460−4464.
(29) Wallace, W. E. Mass Spectra. In *NIST Chemistry WebBook*; Linstrom, P. J., Mallard, W. G., Eds.; NIST Standard Reference Database Number 69; National Institute of Standards and Technology: Gaithersburg MD, 20899, 2021. https://webbook.nist.gov (accessed September 8, 2021).
(30) Pitters, J. L.; Adkinson, D. K.; Griffiths, K.; Norton, P. R.; Workentin, M. S. Chemoselective photochemical surface reaction—Ketene versus carbene reactivity from the photolysis of saturated monolayers of pyridyl diazoesters on single-crystal Pt. *Can. J. Chem.* **2011**, *89*, 117−121.
(31) Hie, L.; Fine Nathel, N. F.; Hong, X.; Yang, Y.-F.; Houk, K. N.; Garg, N. K. Nickel-Catalyzed Activation of Acyl C−O Bonds of Methyl Esters. *Angew. Chem., Int. Ed.* **2016**, *55*, 2810−2814.
(32) Wells, K. D.; McDonald, R.; Ferguson, M. J.; Cowie, M. Unusual Ligand Transformations Initiated by dppm Deprotonation in Methylene-Bridged Rh/Os Complexes. *Inorg. Chem.* **2011**, *50*, 3523−3538.
(33) Sim, W. S.; Gardner, P.; King, D. A. Structure and Reactivity of the Surface Methoxy Species on Ag{111}. *J. Phys. Chem.* **1995**, *99*, 16002−16010.
(34) Sim, W. S.; King, D. A. Surface-Bound Ketenylidene (CCO) from Acetone Decomposition on Ag{111}-*p*(4 × 4)-O. *J. Am. Chem. Soc.* **1995**, *117*, 10583−10584.
(35) Schröder, C.; Schmidt, M. C.; Witt, C.; Attia, S.; Weber, J.; Baumann, A.-K.; Hartke, B.; Schauermann, S. Tuning the Strength of Molecular Bonds in Oxygenates via Surface-Assisted Intermolecular Interactions: Atomistic Insights. *J. Phys. Chem. C* **2020**, *124*, 28159−28168.
(36) Wachs, I. E.; Madix, R. J. The Oxidation of Methanol on a Silver (110) Catalyst. *Surf. Sci.* **1978**, *76*, 531−558.
(37) Zhou, X.-L.; White, J. M.; Koel, B. E. Chemisorption of Atomic Hydrogen on Clean and Cl-Covered Ag(111). *Surf. Sci.* **1989**, *218*, 201−210.
(38) Fleck, L. E.; Ying, Z. C.; Feehery, M.; Dai, H. L. The Adsorption Geometry and Energetics of Formaldehyde Physisorbed on Ag(111): An EELS and TPD Study. *Surf. Sci.* **1993**, *296*, 400−409.
(39) Siau, W.-Y.; Zhang, Y.; Zhao, Y. Stereoselective Synthesis of *Z*-Alkenes. *Top. Curr. Chem.* **2012**, *327*, 33.

https://doi.org/10.1021/acs.jpcc.1c09050
J. Phys. Chem. C 2022, 126, 2482−2492